AGU100 ADVANCING EARTH AND SPACE SCIENCE

Geophysical Research Letters

RESEARCH LETTER
10.1029/2018GL079836

Key Points:
- Summer heat waves (HWs) in eastern Europe (EE) and northern China (NC) are modulated by an intensified mode of variability
- The concurrent variability of HWs in EE and NC is primarily driven by an atmospheric circum-global teleconnection (CGT)
- The GFDL high-resolution atmospheric model shows a poor representation of the EE and NC HWs

Correspondence to:
S. Yang,
yangsong3@mail.sysu.edu.cn

Citation:
Deng, K., Yang, S., Ting, M., Lin, A., & Wang, Z. (2018). An intensified mode of variability modulating the summer heat waves in eastern Europe and northern China. *Geophysical Research Letters*, *45*. https://doi.org/10.1029/2018GL079836

Received 31 JUL 2018
Accepted 8 OCT 2018
Accepted article online 12 OCT 2018

©2018. The Authors.
This is an open access article under the terms of the Creative Commons Attribution-NonCommercial-NoDerivs License, which permits use and distribution in any medium, provided the original work is properly cited, the use is non-commercial and no modifications or adaptations are made.

An Intensified Mode of Variability Modulating the Summer Heat Waves in Eastern Europe and Northern China

Kaiqiang Deng[1], Song Yang[1,2,3], Mingfang Ting[4], Ailan Lin[5], and Ziqian Wang[1]

[1]School of Atmospheric Sciences, Sun Yat-sen University, Guangzhou, China, [2]LASW State Key Laboratory, CMA, Beijing, China, [3]Guangdong Province Key Laboratory for Climate Change and Natural Disaster Studies, Sun Yat-sen University, Guangzhou, China, [4]Lamont-Doherty Earth Observatory, Columbia University, Palisades, NY, USA, [5]Guangzhou Institute of Tropical and Marine Meteorology, CMA, Guangzhou, China

Abstract This study investigates the leading pattern of Eurasian summer heat waves (HWs) using observed and simulated data sets and reveals an intensified mode of variability that bridges the HWs in eastern Europe (EE) and northern China (NC). The concurrent variability of the HWs in EE and NC is primarily driven by an atmospheric circum-global teleconnection that induces anomalous anticyclones over the two regions. The observed upward trends in EE and NC HW days could be related to the warm sea surface temperatures around Greenland Island, which may weaken the Atlantic westerly jet stream and lead to amplified wave trains at the exit of the jet, resulting in strengthened anticyclones over EE and NC that favor the occurrences of HWs. The Geophysical Fluid Dynamics Laboratory high-resolution atmospheric model fails to simulate the EE and NC HWs, due probably to the model's poor representation of the South Asian summer rainfall.

Plain Language Summary Heat waves (HWs) in eastern Europe (EE) and northern China (NC) are found to be bridged via an atmospheric teleconnection, which induces abnormal highs over EE and NC. As a result, the soil conditions in EE and NC become drier and hotter due to the decreased precipitation and increased solar radiation, which favors the occurrences of HWs. The North Atlantic warming may lead to the increases in EE and NC HWs by altering the Atlantic westerly jet stream and associated wave trains. The Geophysical Fluid Dynamics Laboratory high-resolution atmospheric model fails to simulate the EE and NC HWs, due probably to model's poor representation of the South Asian summer rainfall.

1. Introduction

Heat waves (HWs), among the most devastating weather events, are featured by prolonged periods of excessively high temperatures, which could lead to remarkable impacts on human mortality, economies, and ecosystems (e.g., Fouillet et al., 2006; Meehl & Tebaldi, 2004; Poumadère et al., 2005). For example, an extreme HW occurred during July and August of 2010 in eastern Europe (EE) and western Russia, which caused more than 54,000 heat-related deaths in Moscow and provoked thousands of wildfires, making it the most severe heat-related event in history (e.g., Barriopedro et al., 2011; Dole et al., 2011; Grumm, 2011). In the context of global warming, HWs have been reported to become more frequent in the recent decades (Coumou & Rahmstorf, 2012; Deng, Ting, et al., 2018; Perkins et al., 2012) and are expected to become more intense and frequent and last longer in the future warming scenarios (e.g., Christidis et al., 2015; Coumou & Robinson, 2013; Meehl & Tebaldi, 2004), which triggers tremendous interest in the climate community to explore the variability of HWs and associated physical mechanisms.

Eurasia covers around 36.2% of the Earth's total land area and contains over 5 billion people. Previous studies have reported that people in northern Eurasia have suffered through more HWs and droughts since the late half of the 20th century (Schubert et al., 2014; Sillmann et al., 2014). Particularly, the largest increases in HW frequency seem to appear over Europe and East Asia (e.g., Beniston, 2007; Clark et al., 2006), which have resulted in greater socioeconomic losses due to the advanced urbanization and dense population. Although numerous studies have examined the spatial-temporal characteristics of HWs in Europe and East Asia (e.g., Elliot et al., 2014; Otto et al., 2012; Shaposhnikov et al., 2014), most investigations are case analyses. Recently, Wu et al. (2012) and Zhou and Wu (2016) have surveyed the leading pattern of Eurasian summer HWs, which was characterized by an increasing variability centered over Europe and northern China (NC), indicating an intimate linkage of HWs in these two regions. Meanwhile, Lau and Kim (2012) have proposed

an atmospheric teleconnection that may bridge the 2010 Russian HWs and Pakistan floods. In Figures 4a and 4b of Lau and Kim (2012), we have also noticed that the anticyclonic anomaly over Europe coincides with another anticyclonic anomaly over East Asia, suggesting that the concurrent variability of HWs in Europe and East Asia should be tied under specific mechanisms (Trenberth & Fasullo, 2012).

However, the above results are primarily concluded from the 2010 extreme cases, and several questions remain unanswered. For example, is the teleconnection between the European and East Asian HWs robust? Is the intensified variability of European and East Asian HWs a global warming signal or just an interdecadal modulation? The rest of this paper, which addresses the above questions, is organized as follows. Section 2 describes data sets and analysis methods. Section 3 elaborates the results obtained, followed by a summary and discussion in section 4.

2. Data and Methods

We use the daily 2-m temperatures (T2m) from reanalysis products and simulated output by the Geophysical Fluid Dynamics Laboratory (GFDL) global high resolution atmosphere model (HiRAM) to analyze the Eurasian HWs. These data sets include (1) the ERA-Interim (Dee et al., 2011) with a resolution of 1° × 1° during 1979–2016, (2) the ERA-20C (Poli et al., 2016) with a resolution of 1° × 1° during 1900–2010, and (3) an ensemble member of HiRAM with a 50-km horizontal resolution during 1979–2008. The ERA-Interim and ERA-20C data sets are analyzed for the purpose of comparison, which helps to distinguish global warming trend or interdecadal variability in the Eurasian HWs. The HiRAM was developed based on the GFDL Atmospheric Model 2 (AM2) with increased horizontal and vertical resolutions, which is obtained from the experiments forced by observed SST. The HiRAM uses a simpler representation of aerosols than do the AM2 and the AM3 so that it can be run more efficiently at higher resolutions and applies simplified parameterizations for moist convection and large-scale cloudiness, with a goal of providing an improved representation of significant weather events (Harris et al., 2016; Zhao et al., 2009).

Monthly atmospheric data sets are also obtained from the above three data sets, with a resolution of 2.5° × 2.5°, to diagnose the large-scale circulation anomalies associated with the leading mode of Eurasian summer HWs. These variables include the three-dimensional winds, geopotential heights, surface air temperature, and sea level pressure. In addition, monthly precipitation is provided by the CPC Merged Analysis of Precipitation (Xie & Arkin, 1997), with a horizontal resolution of 2.5° × 2.5° for the period of 1979 to present. Monthly mean sea surface temperature (SST) is available from the NOAA Extended Reconstructed SST version 4 (Huang et al., 2015), with a horizontal resolution of 2° × 2° for the period of 1854 to present. The Niño 3.4 index is defined as the mean of monthly normalized SST anomalies at each grid over the area of 170°W–120°W/5°S–5°N, and the circum-global teleconnection (CGT) index is defined by the H200 averaged over northwestern India (35°–40°N/60°–70°E; Ding & Wang, 2005).

A method to determine the relative threshold of T2m is applied in this study (Della-Marta et al., 2007; Deng, Yang, et al., 2018; Kuglitsch et al., 2010). For a specific day within the June-July-August period, a threshold of HWs can be identified by the 95th percentile of ERA-Interim daily T2m for a total of 38 years × 5 days (110 years × 5 days for the ERA-20C; 30 years × 5 days for the HiRAM; the 5 days correspond to 2 days on either side of the target date). By moving the 5-day sample windows forward or backward, we can obtain the consecutive thresholds for every day. An HW event is identified when there are at least 3 consecutive days when the T2m exceeds its 95th percentile threshold. Therefore, the HW day (HWD) for each summer can be acquired. A higher HWD indicates that there are more threshold-breaking hot days or more frequent HWs, and vice versa (Zhou & Wu, 2016). In addition, an empirical orthogonal function (EOF) analysis is employed to capture the first leading mode of Eurasian summer HWD. In regression/correlation analysis, we use the Student's *t* test to assess the statistical significance of the results.

3. Results

3.1. Leading Mode of Eurasian Summer HWD

Figure 1 shows the first EOF mode of Eurasian summer HWD based on observed and simulated data sets. As seen from Figure 1a, the largest variabilities of HWD (ERA-Interim) are mainly concentrated over two regions, that is, EE (30°E–50°E/50°N–60°N) and NC (98°E–118°E/40°N–50°N), which suggests a concurrent variability of

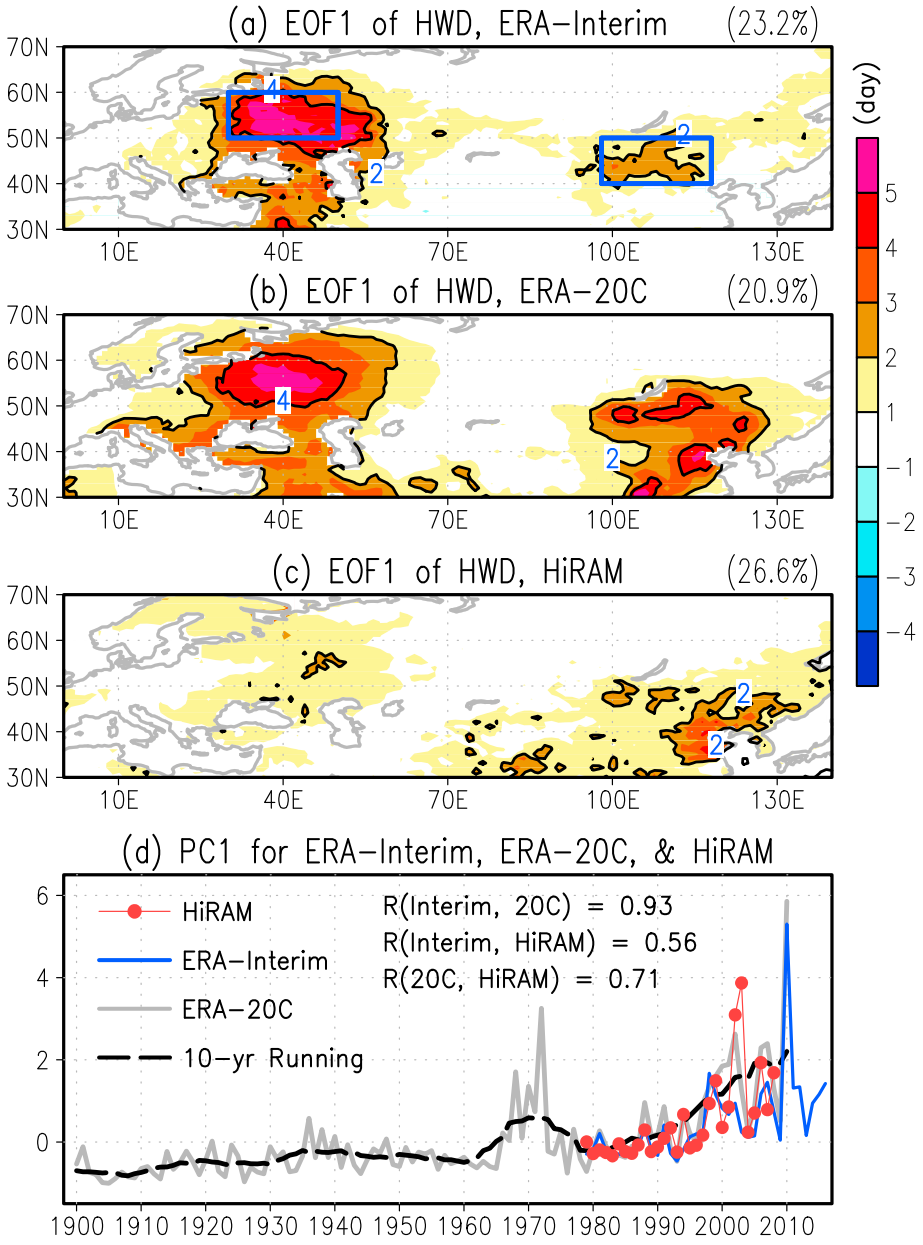

Figure 1. Spatial patterns for the first empirical orthogonal function (EOF) mode of heat wave day (HWD, unit: day) based on the daily 2-m temperatures from the (a) ERA-Interim during 1979–2016, (b) ERA-20C during 1900–2010, and (c) high-resolution atmospheric model during 1979–2008, respectively. (d) Corresponding time series for the first EOF mode of HWD. Eastern Europe (EE, 30°E–50°E, 50°N–60°N) and northern China (NC, 98°E–118°E, 40°N–50°N) are the two key regions of HW's variability, which are outlined by the square boxes in (a).

HWs in these two regions. Figure 1b, obtained from the ERA-20C, displays a similar pattern as Figure 1a, with the strongest signals of HWs over EE and NC. It should be noted that the differences in NC HWs between ERA-Interim (Figure 1a) and ERA-20C (Figure 1b) are considerably large. In fact, these differences still exist when we re-perform the EOF analysis for both data sets over the common period (1979–2010), implying that the differences may result from the reanalysis differences. The ERA-Interim assimilates a wide range of available satellite and in situ observations, and since these observations vary with time, the ERA-Interim is subject to the changes in the input observing systems. By comparison, the ERA-20C assimilates observations of surface pressure and surface marine winds only, and it presumably is not strongly affected by the changes in the input observing systems but is subject to issues in the assimilating model over the

regions that lack abundant surface pressure and marine wind observations (Poli et al., 2016). The first EOF mode of HiRAM-simulated HWD is presented in Figure 1c, where the observed concurrent variability of HWs in EE and NC is generally captured, but the simulated variability in EE and NC HWs is obviously smaller than those in observations.

The time series corresponding to the first EOF mode of HWD are illustrated in Figure 1d. Overall, all of the observed and simulated PC1s have been characterized by consistently upward trends since the 1980s, implying the intensified variabilities and strengthened linkages of HWs in EE and NC. The year-to-year correlation coefficient between PC1 (ERA-Interim) and PC1 (ERA-20C) during 1979–2010 is as high as 0.93. From the PC1 (ERA-20C), it is found that the leading mode of HWD experienced an insignificant trend during 1900s–1970s, suggesting that the intensified mode of variability in Eurasian summer HWs during the recent decades be tied to the recent global warming. The simulated PC1 is significantly correlated with the PC1 (ERA-Interim)/PC1 (ERA-20C), with a correlation coefficient during 1979–2008 of 0.56/0.71, exceeding the 99% confidence level, demonstrating that the HiRAM can, to some extent, reproduce the teleconnection between EE and NC HWs.

Although the concurrent variability of HWs in EE and NC has been clearly revealed in both observations and model simulations, the underlying physical causes are still vague. It is of our interest to explore what mechanisms that may affect the leading mode of Eurasian summer HWs and why the HiRAM shows a weaker representation of the HWs in EE and NC than those in observations.

3.2. Physical Mechanisms for the Leading Mode of Eurasian Summer HWs

To identify the physical causes associated with the leading pattern of Eurasian summer HWs, we analyze the changes in atmospheric circulations by regressing the upper tropospheric stream function and wave activity fluxes (Takaya & Nakamura, 2001) onto the observed and simulated PC1s. As shown in Figures 2a and 2b, anomalous anticyclones are found over EE and NC, corresponding to the concurrent variability of HWs in the two regions. Meanwhile, anomalous cyclones are also observed, which center in central Russia and northwestern India, respectively. The alternative high and low pressure anomalies over Eurasia are actually related to an eastward propagating wave train, which splits into two routes over EE: One continues to propagate northeastward resulting in the central Russian low, and the other propagates southeastward leading to a cyclonic anomaly over northwestern India. As indicated by Figure 2c, the HiRAM has simulated an anticyclone-cyclone-anticyclone circulation pattern over Eurasia. However, the model seems to overstate the northern route of the wave train, reproducing a much stronger cyclonic anomaly over central Russia than those in observations. More importantly, the model seems to fail in simulating the southern route of the wave train, especially the cyclonic anomaly over northwestern India, which may explain why the simulated covariabilities of HWs in EE and NC are smaller compared with the observed. Figures 2d and 2e further show the regression maps of meridional winds onto the PC1s, in a global perspective, to survey the possible sources of variability. The most striking feature is a significant circum-global pattern, whose signals peak in the upstream regions, covering the North Pacific, North America, the North Atlantic, and the Eurasian continent. The correlation coefficient between CGT index and PC1 is 0.50 (ERA-Interim)/0.53 (ERA-20C)/0.22 (HiRAM), implying that the CGT plays a crucial role in modulating the leading pattern of Eurasian summer HWs.

Ding and Wang (2005) have indicated that the South Asian summer monsoon rainfall may affect the CGT pattern by modulating the atmospheric circulation over northwestern India. Therefore, we further examine the precipitation anomalies associated with the concurrent variability of Eurasian summer HWs. As seen from Figures 3a to 3b, the HiRAM-simulated climatic precipitation over southwestern India is obviously less than that in observation. Correlated with the leading mode of Eurasian summer HWs, above-normal precipitation is observed over the Arabian Sea, Iran, and the mountains of Pakistan and Afghanistan (Figure 3c), while the simulated precipitation anomaly over these regions is insignificant and even opposite (Figure 3d). That is, the HiRAM has a difficulty in simulating the observed precipitation pattern over South Asia, which may explain why the HiRAM simulates a weaker linkage of HWs between EE and NC. It should be noted that that the observations used for reanalysis in this part of the world may be poor and, most probably, inhomogeneous in time and space. However, a further examination of the GPCP precipitation reveals a very similar result as the CPC Merged Analysis of Precipitation, indicating that the precipitation pattern is reliable.

Another factor that may affect the CGT is the mean westerly jet stream over the Northern Hemisphere (Ding & Wang, 2005), and model's performance in simulating the jet stream can considerably affect the simulated

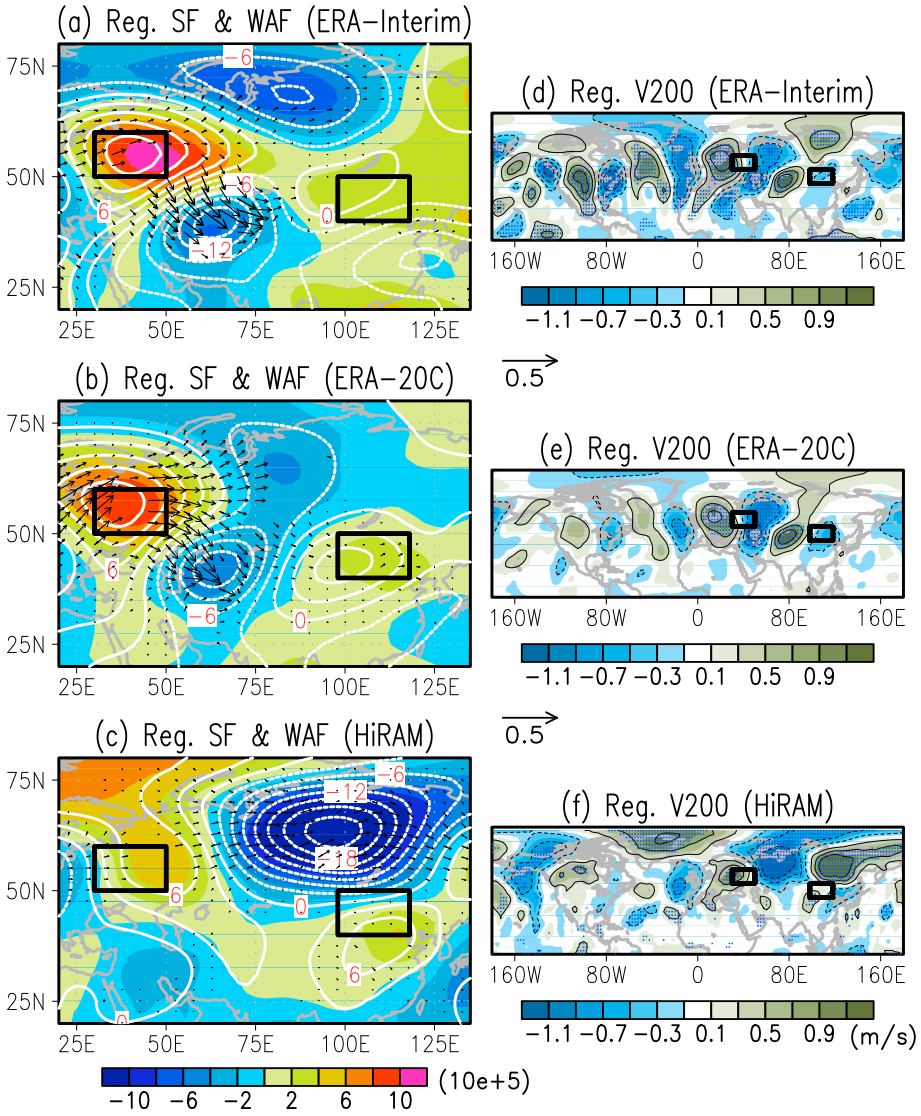

Figure 2. Regression maps of (a) EAR-Interim, (b) ERA-20C, and (c) high resolution atmosphere model 200-hPa stream functions (10^5 m^2 s^{-1}) and Takaya's wave activity fluxes (m^2 s^{-2}) onto the corresponding PC1s (detrended). (d–f) Similar to (a)–(c) except for the 200-hPa meridional wind (V200, m s^{-1}). The areas that exceed the estimated 95% confidence level are stippled in (d)–(f), while the vectors below the 95% confidence level are omitted in (a)–(c). The square boxes in each subplot indicate the locations of eastern Europe and northern China.

CGT pattern and associated anomalies in regional HWs. A further examination reveals that the HiRAM has a good ability in simulating the climatological state of the North Atlantic and Eurasian westerly jet streams (figure not shown). Furthermore, the observed relationship between the upper-level westerly jet streams and the PC1 is also well simulated by the HiRAM, especially over the regions from northern Europe to South Asia, where alternative westerly and easterly anomalies are found. That is to say, the model's performance in simulating the mean flow is relatively reasonable, suggesting that the primary cause for the model's poor representation of the HWs in EE and NC is model's failure in simulating the Indian summer precipitation.

Figure 4 further shows the regression maps of global SSTAs onto the PC1s. Correlated with the PC1s, warming SSTAs appear in the Atlantic, the Indian Ocean, and the northwestern Pacific, coinciding with a cooling SSTA in the eastern Pacific (Figures 4a–4c). After removing the linear trends from the PC1s, as depicted from Figures 4d–4f, the largest changes in SSTAs occur around the Greenland Island, while the eastern Pacific SSTAs seem to become more prominent, reflecting a La Niña-like pattern. Compared with the observations, the HiRAM has simulated a similar SSTA patter as those in observations. Chen et al. (2016) and Chen and Wu

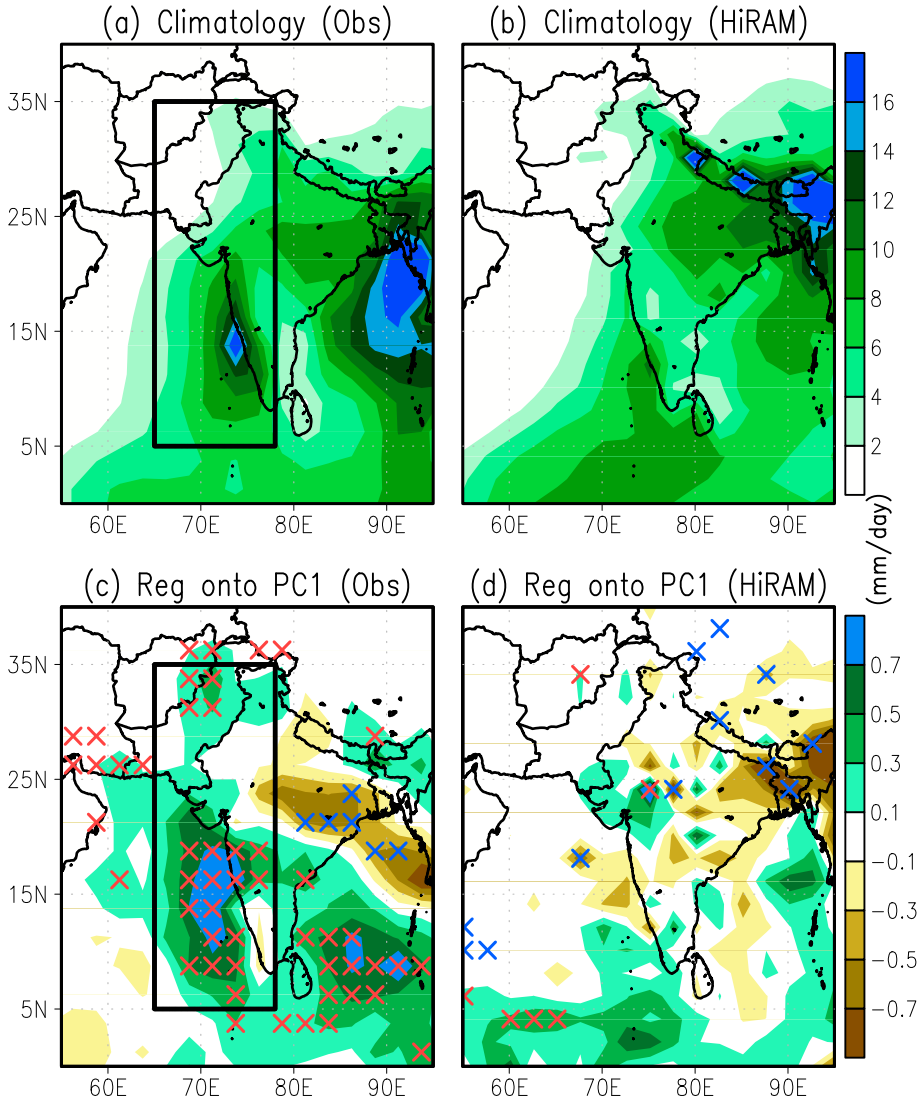

Figure 3. Climatology of June-July-August (JJA) precipitation from (a) CPC Merged Analysis of Precipitation and (b) high resolution atmosphere model data sets (unit: mm/d). (c and d) Similar to (a) and (b) except for the regression maps of JJA precipitation onto the PC1s corresponding to the two data sets. Areas over the estimated 95% confidence level are marked with crosses.

(2017) have indicated that the dominant modes of Eurasian surface air temperature are closely linked to the North Atlantic SSTAs, but their research period is for the boreal spring. Our study further suggests that the recent warming of North Atlantic SST could also connect with the increased frequency of summer HWs in EE and NC. As seen from Figure 4g, an anomalous anticyclone is indeed observed over the warming regions in the North Atlantic, which may induce an anomalous wave train that propagates southeastward, contributing to the significant high pressure over EE. After removing the linear trends (Figure 4h), the anomalous wave train from the Greenland Island disappears, indicating that the North Atlantic SSTAs may play some roles in modulating the trends in EE and NC HWs.

It should be cautious that the North Atlantic warm SSTs could be a response to the atmosphere rather than a direct forcing, as the high-latitude SSTs may be insufficient to trigger the deep convection that affects the upper-level atmosphere. In fact, the intensified anticyclones in the high latitudes often correspond to anomalously descending motions and increased solar radiation that may warm the SST. Nevertheless, the North Atlantic warm SSTs may indirectly affect the CGT-related wave trains through weakening the North Atlantic westerly jet stream (NAWJS). That is, the widespread warming around the Greenland Island can

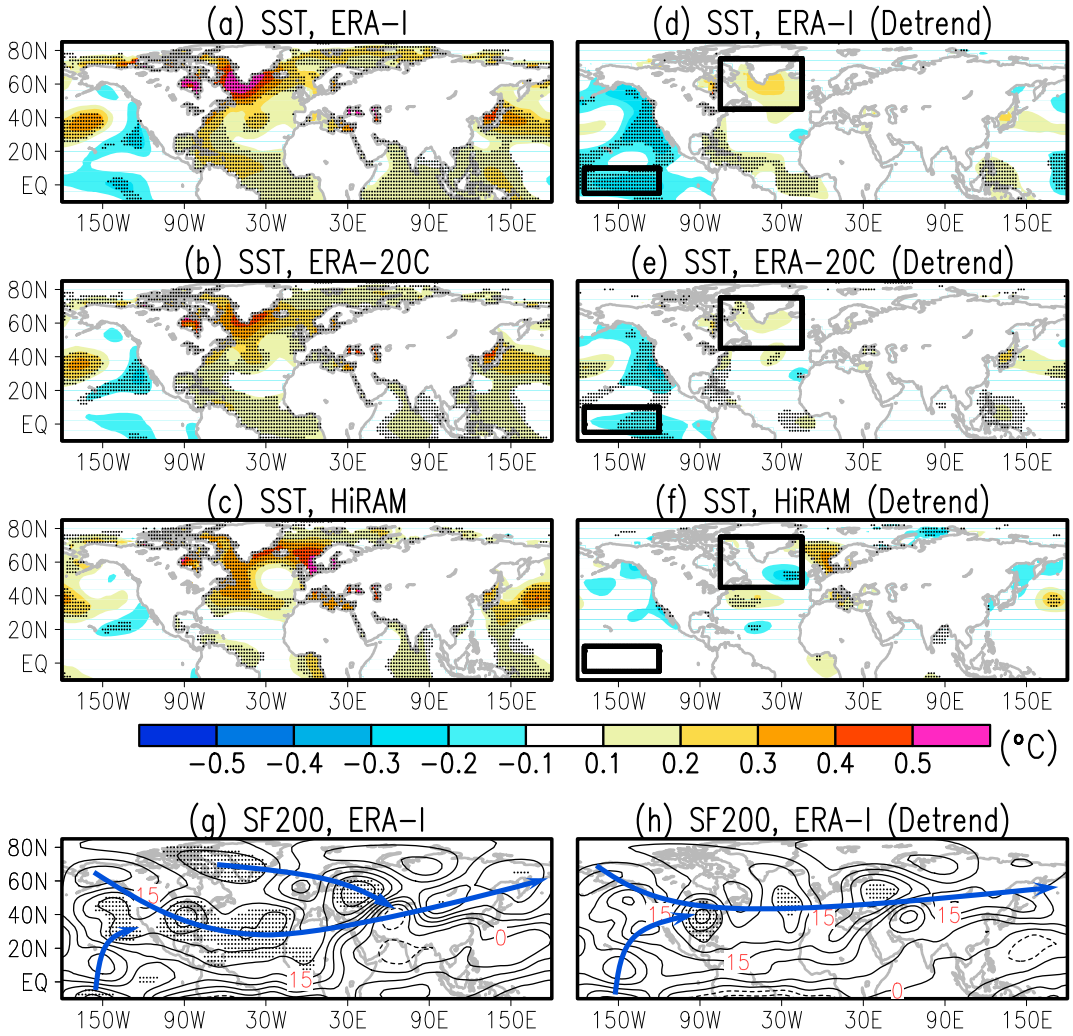

Figure 4. Regression of NOAA-ER4 JJA sea surface temperature (unit: °C) onto the corresponding PC1s obtained from (a) EAR-Interim, (b) ERA-20C, and (c) high resolution atmosphere model, respectively. (g) Regression of ERA-Interim 200-hPa stream function (SF200, 10^5 m^2 s^{-1}) onto the corresponding PC1. The right panels are similar as the left except for the removal of linear trends from PC1s. Areas exceeding the 95% confidence levels are stippled.

reduce the local meridional SST gradient and subsequently cause a slower NAWJS. As a result, the atmospheric wave trains could strengthen at the exit of the jet, leading to the intensified anticyclones over EE and NC. Therefore, the North Atlantic warm SSTs may connect the EE and NC HWs through indirect ways, that is, modulations of the NAWJS as well as the CGT-related wave trains.

4. Summary and Discussion

This study has investigated the leading pattern of Eurasian summer HWs. A concurrent variability of HWs in EE and NC is found from observations and model simulations, which show an upward trend during the past several decades. Although the atmospheric model has generally reproduced the leading pattern of Eurasian summer HWs, the simulated variability of HWs in EE and NC is obviously smaller than that in observations, due probably to the model's poor representation of the South Asian summer rainfall. The concurrent variations of HWs in EE and NC are primarily driven by the atmospheric CGT, which induces anomalous anticyclones over EE and NC. The increasing trends in EE and NC summer HW days could be related to the recent warming of the North Atlantic, which reduces the local meridional SST gradient and subsequently causes a slower westerly jet stream over the North Atlantic. As a result, the CGT-related wave trains may be strengthened at the exit of the jet stream, leading to the intensified anticyclones over EE and NC.

Under the control of anomalous anticyclones, significant descending motions occur over EE and NC, which on the one hand prohibit the formation of cloud, and on the other hand suppress convection. The reduced cloud cover increases the solar radiation at the surface, while the suppressed convection and decreased precipitation may cause a drier and hotter soil condition in favor of the HWs in these regions. It should be noted that the warm SSTAs around the Greenland Island may reflect a global warming footprint due to the increased anthropogenic CO_2 emission and/or result from the recent phase shift of the Atlantic Multidecadal Oscillation, which deserves further investigations.

Acknowledgments
This study was supported by the National Key Research and Development Program of China (2016YFA0602703), the National Key Scientific Research Plan of China (grant 2014CB953904), the National Natural Science Foundation of China (grants 41690123, 41690120, 91637208, and 41661144019), the "111-Plan" Project of China (grant B17049), the LASW State Key Laboratory Special Fund (2016LASW-B01), the Science and Technology Planning Project of Guangzhou (grant 201704020194), and the CMA Guangzhou Joint Research Center for Atmospheric Sciences. We acknowledge the GFDL, which is responsible for the high-resolution atmospheric model experiment. We are grateful to the European Centre for Medium-Range Weather Forecasts for archiving the reanalysis data.

References

Barriopedro, D., Fisher, E. M., Luterbacher, J., Trigo, R. M., & Garcie-Herrera, R. (2011). The hot summer of 2010: Redrawing the temperature record map of Europe. *Science*, *332*(6026), 220–224. https://doi.org/10.1126/science.1201224

Beniston, M. (2007). Entering into the "greenhouse century": Recent record temperatures in Switzerland are comparable to the upper temperature quantiles in a greenhouse climate. *Geophysical Research Letters*, *34*, L16710. https://doi.org/10.1029/2007GL030144

Chen, S. F., & Wu, R. G. (2017). Interdecadal changes in the relationship between interannual variations of spring North Atlantic SST and Eurasian surface air temperature. *Journal of Climate*, *30*(10), 3771–3787. https://doi.org/10.1175/JCLI-D-16-0477.1

Chen, S. F., Wu, R. G., & Liu, Y. (2016). Dominant modes of interannual variability in Eurasian surface air temperature during boreal spring. *Journal of Climate*, *29*(3), 1109–1125. https://doi.org/10.1175/JCLI-D-15-0524.1

Christidis, N., Jones, G. S., & Stott, P. A. (2015). Dramatically increasing chance of extremely hot summers since the 2003 European heatwave. *Nature Climate Change*, *5*(1), 46–50. https://doi.org/10.1038/nclimate2468

Clark, R. T., Brown, S. J., & Murphy, J. M. (2006). Modeling Northern Hemisphere summer heat extreme changes and their uncertainties using a physics ensemble of climate sensitivity experiments. *Journal of Climate*, *19*(17), 4418–4435. https://doi.org/10.1175/JCLI3877.1

Coumou, D., & Rahmstorf, S. (2012). A decade of weather extremes. *Nature Climate Change*, *2*, 491–496. https://doi.org/10.1038/nclimate1452

Coumou, D., & Robinson, A. (2013). Historic and future increase in the global land area affected by monthly heat extremes. *Environmental Research Letters*, *8*(3), 034018. https://doi.org/10.1088/1748-9326/8/3/034018

Dee, D. P., Uppala, S. M., Simmons, A. J., Berrisford, P., Poli, P., Kobayashi, S., et al. (2011). The ERA-Interim reanalysis: Configuration and performance of the data assimilation system. *Quarterly Journal Of The Royal Meteorological Society*, *137*(656), 553–597. https://doi.org/10.1002/qj.828

Della-Marta, P. M., Haylock, M. R., Luterbacher, J., & Wanner, H. (2007). Doubled length of western European summer heat waves since 1880. *Journal of Geophysical Research*, *112*, D15103. https://doi.org/10.1029/2007JD008510

Deng, K. Q., Ting, M. F., Yang, S., & Tan, Y. H. (2018). Increased frequency of summer extreme heat waves over Texas area tied to the amplification of Pacific zonal SST gradient. *Journal of Climate*. https://doi.org/10.1175/JCLI-D-17-0554.1

Deng, K. G., Yang, S., Ting, M. F., Tan, Y. H., & He, S. (2018). Global monsoon precipitation: trends, leading modes, and associated drought and heat wave in the Northern Hemisphere. *Journal of Climate*. https://doi.org/10.1175/JCLI-D-17-0569.1

Ding, Q. H., & Wang, B. (2005). Circumglobal teleconnection in the Northern Hemisphere summer. *Journal of Climate*, *18*(17), 3483–3505. https://doi.org/10.1175/JCLI3473.1

Dole, R., Hoerling, M., Perlwitz, J., Eischeid, J., Pegion, P., Zhang, T., et al. (2011). Was there a basis for anticipating the 2010 Russian heat wave? *Geophysical Research Letters*, *38*, L06702. https://doi.org/10.1029/2010GL046582

Elliot, A. J., Bone, A., Morbey, R., Hughes, H. E., Harcourt, S., Smith, S., et al. (2014). Using real-time syndromic surveillance to assess the health impacts of the 2013 heatwave in England. *Environmental Research Letters*, *135*, 31–36. https://doi.org/10.1016/j.envres.2014.08.031

Fouillet, A., Rey, G., Laurent, F., Pavillon, G., Bellec, S., Guihenneuc-Jouyaux, C., et al. (2006). Excess mortality related to the August 2003 heat wave in France. *International Archives of Occupational and Environmental Health*, *80*(1), 16–24. https://doi.org/10.1007/s00420-006-0089-4

Grumm, R. H. (2011). The central European and Russian heat event of July–August 2010. *Bulletin of the American Meteorological Society*, *92*(10), 1285–1296. https://doi.org/10.1175/2011BAMS3174.1

Harris, L. M., Lin, S.-J., & Tu, C. Y. (2016). High-resolution climate simulations using GFDL HiRAM with a stretched global grid. *Journal of Climate*, *29*(11), 4293–4314. https://doi.org/10.1175/JCLI-D-15-0389.1

Huang, B., Banzon, V. F., Freeman, E., Lawrimore, J., Liu, W., Peterson, T. C., et al. (2015). Extended Reconstructed Sea Surface Temperature version 4 (ERSST.v4). Part I: Upgrades and intercomparison. *Journal of Climate*, *28*(3), 911–930. https://doi.org/10.1175/JCLI-D-14-00006.1

Kuglitsch, F. G., Toreti, A., Xoplaki, E., Della-Marta, P. M., Zerefos, C. S., Türkeş, M., & Luterbacher, J. (2010). Heat wave changes in the eastern Mediterranean since 1960. *Geophysical Research Letters*, *37*, L04802. https://doi.org/10.1029/2009GL041841

Lau, K. M., & Kim, K.-M. (2012). The 2010 Pakistan flood and Russian heat wave: Teleconnection of hydrometeorological extremes. *Journal of Hydrometeorology*, *13*(1), 392–403. https://doi.org/10.1175/JHM-D-11-016.1

Meehl, G. A., & Tebaldi, C. (2004). More intense, more frequent, and longer lasting heat waves in the 21st century. *Science*, *305*(5686), 994–997. https://doi.org/10.1126/science.1098704

Otto, F. E. L., Massey, N., van Oldenborgh, G. J., Jones, R. G., & Allen, M. R. (2012). Reconciling two approaches to attribution of the 2010 Russian heat wave. *Geophysical Research Letters*, *39*, L04702. https://doi.org/10.1029/2011GL050422

Perkins, S. E., Alexander, L. V., & Nairn, J. (2012). Increasing frequency, intensity and duration of observed global heat waves and warm spells. *Geophysical Research Letters*, *39*, L20714. https://doi.org/10.1029/2012GL053361

Poli, P., Hersbach, H., & Dee, D. P. (2016). ERA-20C: An atmospheric reanalysis of the 20th century. *Journal of Climate*, *29*(11), 4083–4097. https://doi.org/10.1175/JCLI-D-15-0556.1

Poumadère, M., Mays, C., Le Mer, S., & Blong, R. (2005). The 2003 heat wave in France: Dangerous climate change here and now. *Risk Analysis*, *25*(6), 1483–1494. https://doi.org/10.1111/j.1539-6924.2005.00694.x

Schubert, S. D., Wang, H., Koster, R. D., Suarez, M. J., & Groisman, P. Y. (2014). Northern Eurasian heat waves and droughts. *Journal of Climate*, *27*(9), 3169–3207. https://doi.org/10.1175/JCLI-D-13-00360.1

Shaposhnikov, D., Revich, B., Bellander, T., Bedada, G. B., Bottai, M., Kharkova, T., et al. (2014). Mortality related to air pollution with the Moscow heat wave and wildfire of 2010. *Epidemiology*, *25*(3), 359–364. https://doi.org/10.1097/EDE.0000000000000090

Sillmann, J., Donat, M. G., Fyfe, J. C., & Zwiers, F. W. (2014). Observed and simulated temperature extremes during the recent warming hiatus. *Environmental Research Letters*, *9*(6), 064023. https://doi.org/10.1088/1748-9326/9/6/064023

Takaya, K., & Nakamura, H. (2001). A formulation of a phase-independent wave-activity flux for stationary and migratory quasigeostrophic eddies on a zonally varying basic flow. *Journal of the Atmospheric Sciences*, *58*(6), 608–627. https://doi.org/10.1175/1520-0469(2001)058<0608:AFOAPI>2.0.CO;2

Trenberth, K. E., & Fasullo, J. T. (2012). Climate extremes and climate change: The Russian heat wave and other climate extremes of 2010. *Journal of Geophysical Research*, *117*, D17103. https://doi.org/10.1029/2012JD018020

Wu, Z., Jiang, Z., Li, J., Zhong, S., & Wang, L. (2012). Possible association of the western Tibetan Plateau snow cover with the decadal to interdecadal variations of northern China heatwave frequency. *Climate Dynamics*, *39*(9-10), 2393–2402. https://doi.org/10.1007/s00382-012-1439-4

Xie, P., & Arkin, P. A. (1997). Global precipitation: A 17-year monthly analysis based on gauge observations, satellite estimates, and numerical model outputs. *Bulletin of the American Meteorological Society*, *78*(11), 2539–2558. https://doi.org/10.1175/1520-0477(1997)078<2539:GPAYMA>2.0.CO;2

Zhao, M., Held, I. M., Lin, S.-J., & Vecchi, G. A. (2009). Simulations of global hurricane climatology, interannual variability, and response to global warming using a 50-km resolution GCM. *Journal of Climate*, *22*(24), 6653–6678. https://doi.org/10.1175/2009JCLI3049.1

Zhou, Y., & Wu, Z. (2016). Possible impacts of mega-El Niño/Southern Oscillation and Atlantic Multidecadal Oscillation on Eurasian heatwave frequency variability. *Quarterly Journal Of The Royal Meteorological Society*, *142*(697), 1647–1661. https://doi.org/10.1002/qj.2759